ISIJ International, Vol. 30 (1990), No. 3, pp. 233-240

Resistance Spot Weldability of Comparatively Thick C–Mn–Cr–Mo Dual Phase Steel Sheet

P.K. GHOSH,[1] P.C. GUPTA,[1] Ram AVTAR[2] and B.K. JHA[2]

1) Welding Research Laboratory, Department of Mechanical & Industrial Engineering, University of Roorkee, Roorkee 247 667, India.
2) RDCIS, Steel Authority of India, Ltd., Ranchi 834 002, India.

(Received on May 29, 1989; accepted in the final form on September 8, 1989)

Welding of comparatively thick (4 mm) C–Mn–Cr–Mo dual phase steel has been carried out by resistance spot welding process. Weldability of this steel has been studied by varying the electrode force and the primary welding parameters affecting the heat input such as the effective current and weld time. The influence of these welding parameters on the morphology, microhardness and the tensile shear strength of the weldment are investigated. Optimum welding parameters producing maximum joint strength are established as electrode force of 615 kg, effective current of 6 kA and weld time of 80 cycle. Weakening of weldment caused by excess tempering of martensite at the outer region of HAZ was not observed in the range of optimum welding conditions.

KEY WORDS: C–Mn–Cr–Mo dual phase steel; 4 mm thick sheet; resistance spot welding; tensile shear strength; microhardness; microstructure.

1. Introduction

Dual phase steel is a new class of high strength low alloy steel having microstructure of strong martensite and/or bainite colonies dispersed in soft matrix of ferrite.[1,2] It is well known that this steel is having a number of unique properties such as absence of yield point, low yield/tensile strength ratio, high work hardening rate and high uniform elongation.[1–4] The last two properties indicate the presence of excellent formability which, coupled with its high tensile strength, has made this steel attractive for weight saving applications especially in automobile industries for greater fuel economy.[1,3,5] But the wide acceptance of dual phase steel in automobile industries is still not appreciable due to insufficient knowledge regarding its weldability under different welding processes.

For automotive applications it is imperative for the material to posses a good spot weldability and this is to a great extent dependent on the plate thickness, morphology of base metal and its mechanical properties.[6,7] The morphology and properties of base metal are governed by its chemical composition and production process. Further the chemical composition and morphology of base metal dictate the weldability of dual phase steel by affecting the transformation behaviour at heat affected zone (HAZ). In past few years a considerable amount of effort has been made to study the resistance spot weldability of 0.8–3.0 mm thick dual phase steel of various chemical compositions such as C–Mn, C–Mn–Si–Al, C–Mn–Nb(V), and C–Mn–Mo.[6–14] However, a comparatively thicker dual phase steel, having thickness of the order of 4.0 mm, have also received attention from automobile industries and some work is reported on spot weldability of so thick C–Mn–Si–V dual phase steel.[6] Besides the dual phase steels of various chemical compositions mentioned above, the C–Mn–Cr–Mo dual phase steel has also been gathered a considerable acceptance by the automobile industries[15] and an effort has already been made to study the weldability of this material in comparatively low range of thickness of the order of 2.5 mm.[16]

Looking forward to a potential demand of comparatively thick C–Mn–Cr–Mo dual phase steel plate in fabrication of heavy surface transport vehicle, an effort has been made in the present work to investigate the weldability of this steel having thickness of the order of 4.0 mm under resistance spot welding process.

2. Experimentation

2.1. Welding Procedure

The 4.0 mm thick hot rolled dual phase steel plates having chemical composition given in Table 1 was resistance spot welded in a pneumatic phase shift controlled AC spot welding machine of capacity 184 kVA. Before welding the surface of the specimen was mechanically cleaned and the welding was carried out by using water cooled conical Cu–Cr alloy electrode having contact surface of 11.0 mm in diameter.

Table 1. Chemical composition of base plate.

Chemical composition (wt%)						
C	Mn	Si	Cr	Mo	S	P
0.08	1.2	1.0	0.45	0.34	0.02	0.02

Typical welded specimen prepared for tensile shear test, by over lapping the plates, has been shown in Fig. 1. During welding at a given holding time the various parameters such as the effective current, weld time and electrode force were varied as shown in Table 2. The values of weld time and holding time are presented in an unit of " cycle " where, 100 cycle represents a time of 1 s. The effective current during welding was measured with the help of a weld current monitor having a range upto 200 kA and the weld time and electrode force were varied, as desired, by adjusting the facilities available in the machine. The welding process has been shown schematically in Fig. 2, where the pause time is equal to the weld time.

2.2. *Tensile Test*

The tensile property of base plate was determined by using standard (DIN 50 120) flat tensile specimen. The tensile test of base plate and the tensile shear test of welded specimens were carried out in microprocessor controlled servohydraulic universal testing machine at a cross head speed of 1 mm/min.

2.3. *Metallography*

The transverse section of base plate and that of the weld passing through its centre were prepared by standard metallographic procedure and etched with alcoholic nitric acid. The specimens were studied under optical and scanning electron microscopes.

2.4. *Microhardness Study*

The microhardness measurement across the weld and of base metal was carried out on the metallographic specimens at a load of 100 g. The indentation was randomly made on the matrix without marking the specific phases. However, in case of welded specimen attention was paid for indentation in the region identified as weld centre and the locations where a distinct change in microstructure was marked.

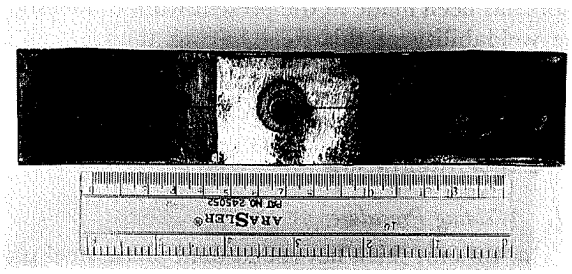

Fig. 1. Photograph of a typical tensile shear test sample.

3. Results and Discussion

3.1. *Properties of Base Plate*

The mechanical properties of base plate have been shown in Table 3. The typical microstructure of the hot rolled dual phase steel plate revealed under optical and scanning electron microscope are shown in Figs. 3(a) and 3(b), respectively. In Fig. 3(a) the comparatively darker regions are the martensite colonies in ferrite matrix where as in Fig. 3(b) the

Table 2. Mechanical properties of the base plate.

UTS (kg/mm²)	Y. S. (kg/mm²)	Elongation (%)	Microhardness (VHN)
70.6	52.0	18.0	245

Table 3. Scheme of the welding parameters and their performance.

Effective current (kA)	Weld time (cycle)	Electrode force (kg)	Remakrs/Observations	
			During welding	Region of failure during tensile shear test
5.0	30	615	—	Interface
5.0	40	615	—	ditto
5.0	50	615	—	ditto
5.0	60	615	—	ditto
5.0	80	615	—	ditto
5.0	90	615	—	ditto
6.0	20	615	—	ditto
6.0	40	615	—	ditto
6.0	50	615	—	ditto
6.0	60	615	—	ditto
6.0	80	615	—	ditto
6.0	90	615	—	ditto
6.8	20	615	Expulsion	ditto
6.8	40	615	ditto	ditto
6.8	50	615	ditto	ditto
6.8	60	615	ditto	ditto
6.8	80	615	ditto	Outer region of HAZ
6.8	90	615	ditto	ditto
7.4	50	615	ditto	Interface
6.0	80	440	ditto	ditto
6.0	80	500	ditto	ditto
6.0	80	700	—	ditto

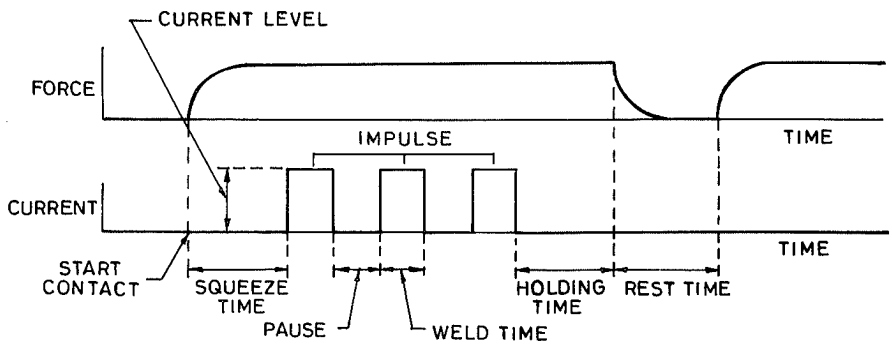

Fig. 2.
Schematic diagram of the resistance spot welding process.

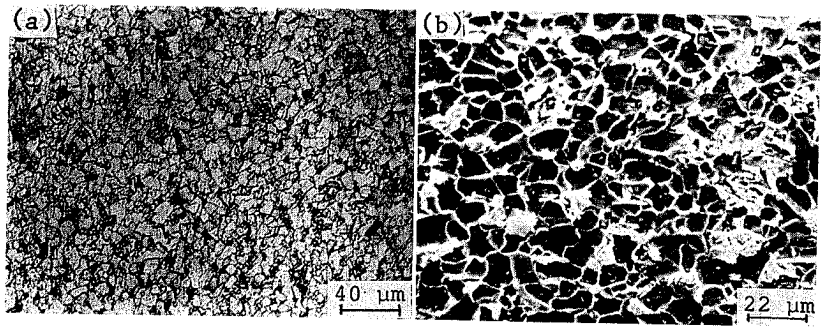

Fig. 3.
Microstructure of base metal revealed under (a) optical and (b) scanning electron microscopes.

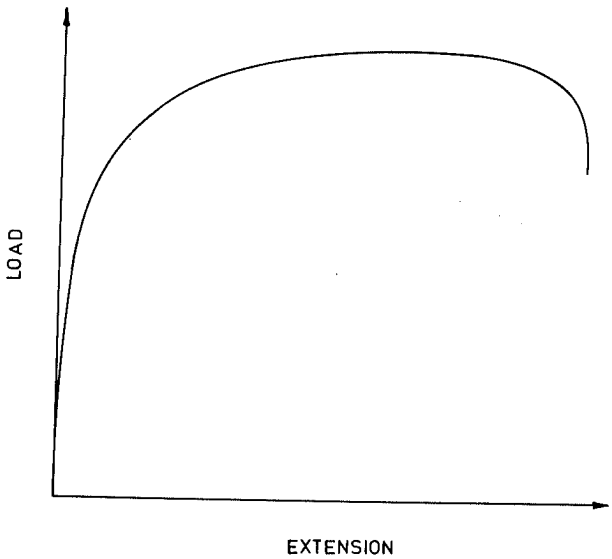

Fig. 4. Typical tensile load *vs.* extension plot of the base material.

martensite colonies are revealed as white region in comparatively dark ferrite matrix. The typical continuous yielding behaviour of the material as shown in the tensile load *vs.* extension plot of base plate, presented in Fig. 4 identifies the characteristics of its dual phase matrix.

3.2. *General Concept and Visual Observations*

The mechanical properties of a spot weld depend primarily on (i) size and hardness of nugget, (ii) depth of electrode impression on the weld surface causing the thinning of nugget, and (iii) microstructure of HAZ governing its strength and ductility. However, the strength of a spot weld is competitive in nature between the load bearing capacity of nugget and that of HAZ. To achieve maximum strength a spot weld must have a nugget size large enough to provide greater resistance to fracture as compared to the same offered by HAZ whichever is stronger. Unlike that observed in case of spot welding of plain carbon steel,[17] during spot welding of thin dual phase steel sheet of thickness of the order of 3.0 mm, always there is a possibility to form a comparatively weak region of tempered martensite at the outer region of HAZ[18] where probably the temperature rises upto about 600–650°C.[5,19] This tempered martensite region has been found to be even weaker than the base metal.[18,19]

The morphology of weld and HAZ governing its strength and ductility is primarily controlled by the weld thermal cycle which in turn is controlled by the energy input resulting primarily from effective welding current and time. The reduction in energy input decreases the nugget size where as an excessive energy input causes coarsening of weld and HAZ microstructures. Moreover, at a given electrode force the use of an excessive energy input or at a given energy input the use of too low an electrode force results in expulsion from weld nugget and weakens the same. In present investigation the welding parameters at which the expulsion takes place have been shown in Table 2. The table shows that the expulsion occurs at the effective current of 6.8 kA and more or at an effective current of 6.0 kA when the electrode force is 500 kg or less. In case of expulsion generally the weld has been found to fail from the interface. However, the mode of fracture is marked predominantly of ductile nature.

3.3. *Influence of Effective Current and Weld Time*

The effective current and weld time are the primary welding parameters affecting the weld thermal cycle. At different levels of weld time as 40, 50, and 80 cycle the influence of variation in effective current from 5 to 7.4 kA on the ultimate tensile shear load bearing capacity of the weld has been shown in Fig. 5. Similarly at different levels of effective current as 5, 6 and 6.8 kA the influence of variation in wled time from 20 to 90 cycle on the ultimate tensile shear load bearing capacity of the weld has been shown in Fig. 6. The increase in energy input caused by an enhancement in effective current and weld time increases the nugget size of the weld. In case of increase in welding parameters such as the effective current and weld time as mentioned in Figs. 5 and 6, respectively, the observed enhancement in nugget size are depicted in Figs. 7 and 8, respectively. The increase in energy input also coarsens the microstructure of weld nugget as well as that of HAZ (close to weld nugget) as revealed in the micrographs presented in Figs. 9 and 10, respectively, where at a given weld time of 50 cycle the effective current has been increased from 6 upto 7.4 kA.

The increase in nugget size with the increase in energy input (Figs. 7 and 8) has been found primarily to enhance the strength of weldment as shown in Figs. 5 and 6, where at a given weld time the effective current and at a given effective current the weld time are varied, respectively. The above phenomena has

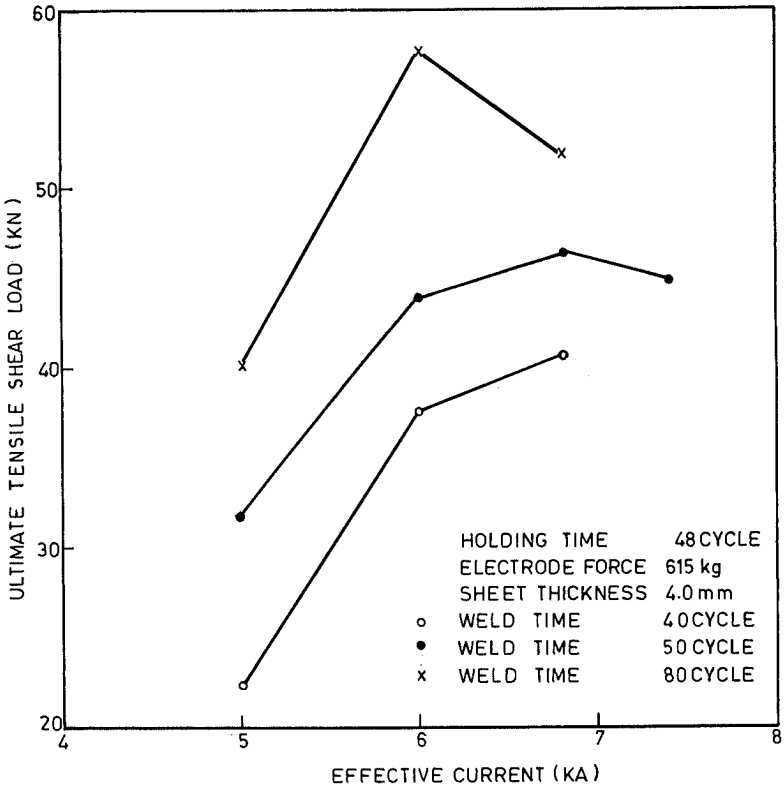

Fig. 5.
Influence of variation in effective current on the ultimate tensile shear load bearing capacity of the weld.

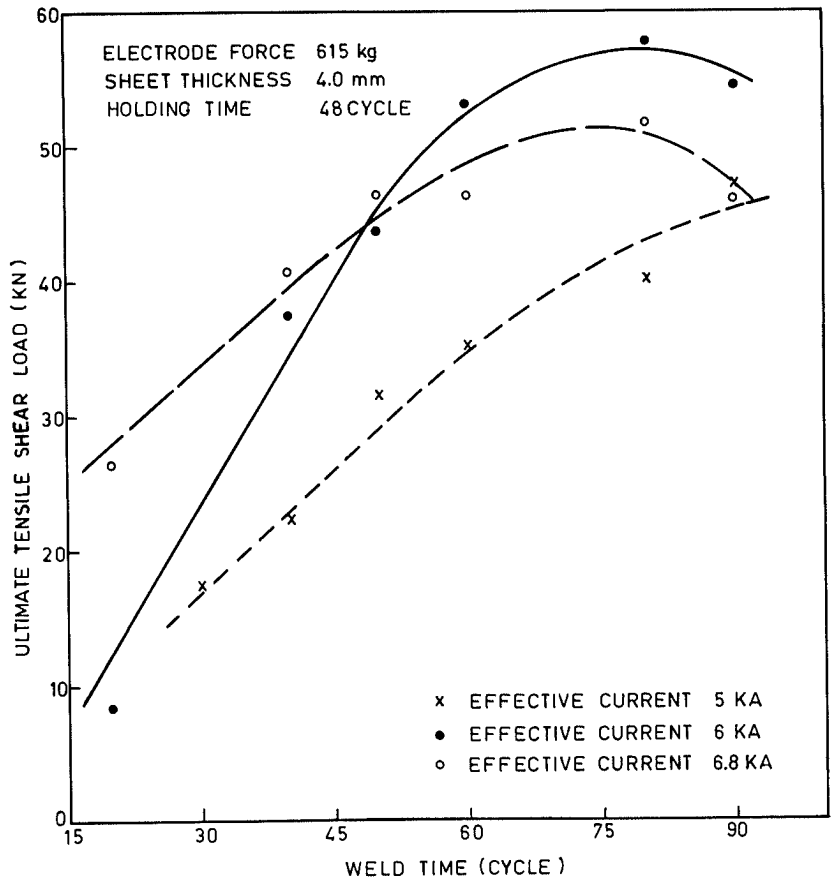

Fig. 6.
Influence of variation in weld time on the ultimate tensile shear load bearing capacity of the weld.

been found effective when at a given weld time upto 50 cycle the effective current is raised upto 6.8 kA and at the weld time of 80 cycle the effective current is raised upto 6 kA (Fig. 5). Similarly the same phenomena has been found to work when at a comparatively low effective current of 5 kA the weld time is increased upto 90 cycle and at the effective currents of 6 and 6.8 kA the weld time is raised upto 80 cycle (Fig. 6). The increase in energy input coarsens the accicular ferrite of weld nugget (Fig. 9) and thus, weakens this region as depicted in the microhardness study carried out on these welds, shown in Fig. 11.

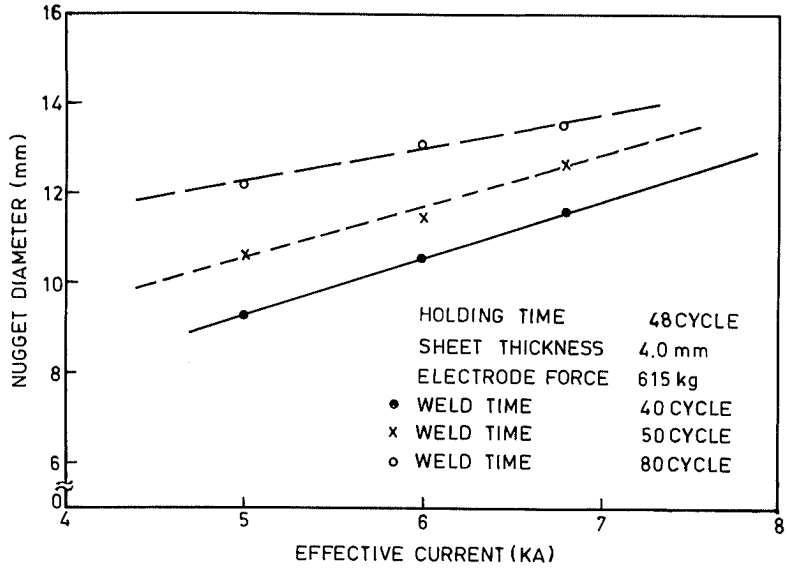

Fig. 7.
Influence of variation in effective current on the nugget size.

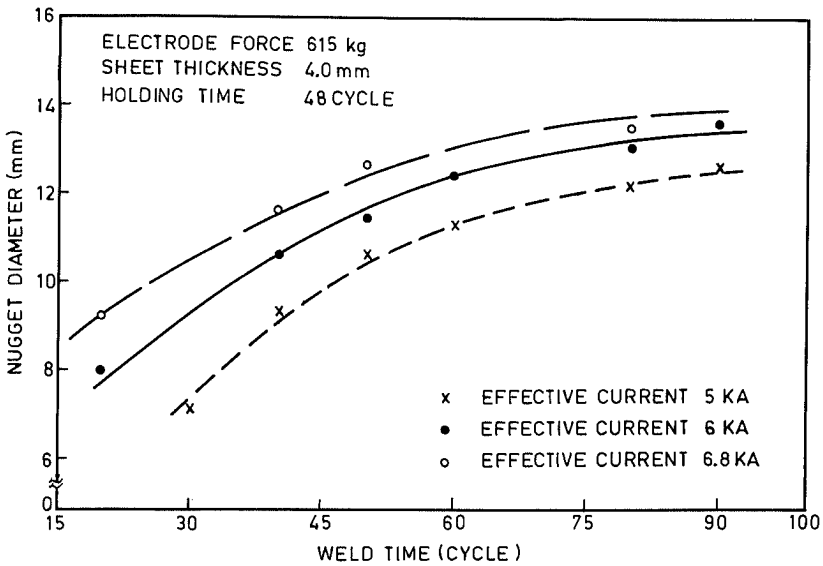

Fig. 8.
Influence of variation in weld time on the nugget size.

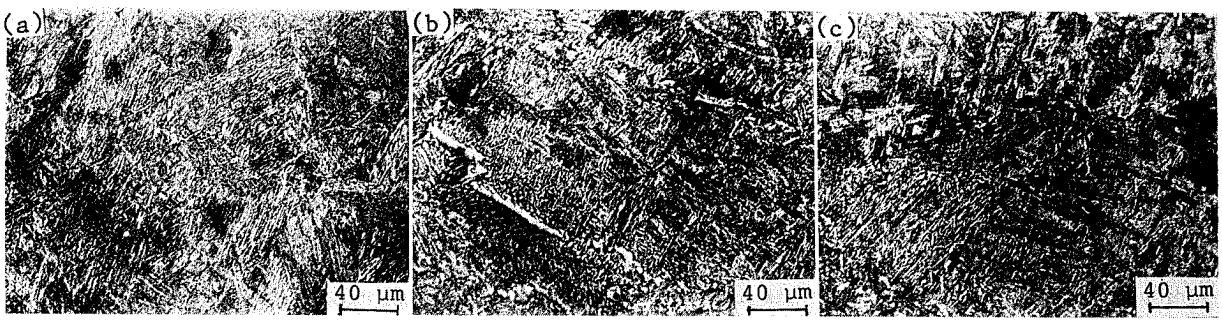

Fig. 9. Influence of effective current on the microstructure of weld nugget, (a) 6 kA; (b) 6.8 kA; (c) 7.4 kA.

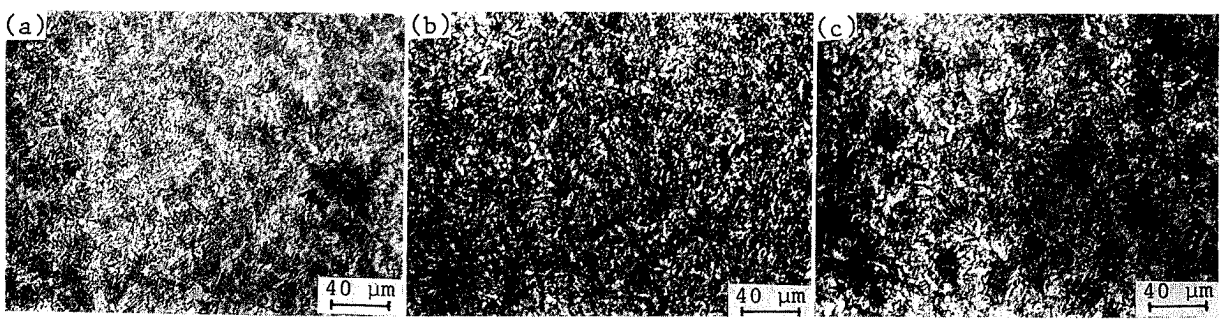

Fig. 10. Influence of effective current on the microstructure of HAZ close to the weld nugget, (a) 6 kA; (b) 6.8 kA; (c) 7.4 kA.

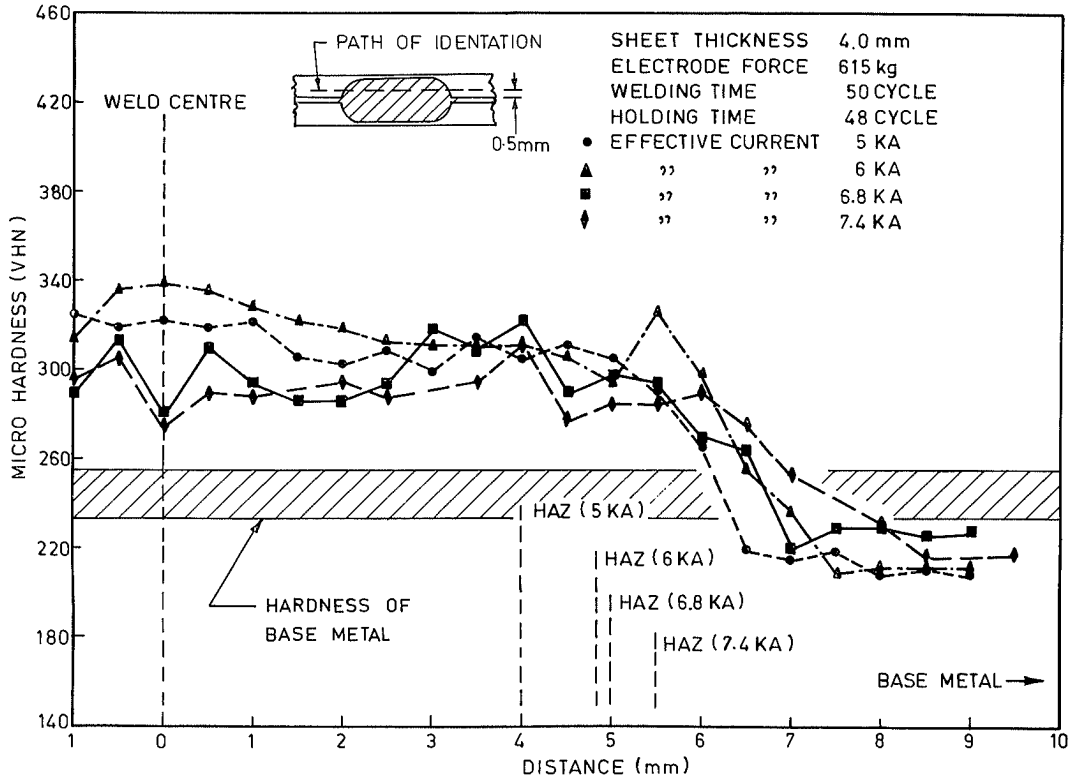

Fig. 11. Microhardness across the weld prepared at different effective current, welding time=50 cycle.

At an effective current of 6 kA the reduction of nugget strength (interface failure, Table 2) with a further increase in weld time beyond 80 cycle (Fig. 6) may have been caused by the excessive coarsening of microstructure of the nugget. The base plate used in this work is comparatively thicker (4 mm). So, in case of all the combination of parameters concerning the effective current and weld time the weld has been found to fail from the interface, which is further substantiated by the expulsion occurred during the use of effective currents of the order of 6.8 and 7.4 kA (Table 2). The creation of nugget defect caused by the expulsion may have primarily restricted the weld strength to a comparatively low level (Fig. 6) inspite of its higher nugget size (Fig. 8) when the effective current of 6.8 kA is used. But it is interesting to note that at the effective current of 6.8 kA when the weld time is raised to 80 cycle and above, inspite of weakening of the nugget due to defective welding caused by significant expulsion the weldment has not failed from the interface rather from the outer region of HAZ (Table 2) defined as a zone where a considerable change in microstructure is marked. In agreement to the earlier work[18] of similar nature here also the failure has been found to occur from the outer region of HAZ. This may have occurred due to significant weakening of HAZ resulted from the coarsening of its microstructure at a comparatively high energy input along with a considerable tempering of martensite marked at its outer region as typically depicted in Fig. 12. The tempering of martensite may always occur at the outer region of HAZ where the temperature during welding possibly lies in the range of 600–650°C[5,19] and results into weakening of

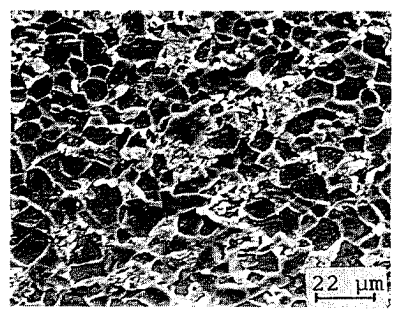

Fig. 12. Typical scanning electron micrograph of tempering of martensite at the outer region of HAZ.

this region as it is observed in its microhardness behaviour shown in Fig. 11. The increase in energy input possibly allows this region to stay for a larger time at the tempering temperature range and causes a substantial weakening leading to an early failure. The results presented in Figs. 5 and 6 show that the weldment prepared at the effective current and weld time of 6 kA and 80 cycle respectively possesses the maximum ultimate tensile shear strength. The microstructure of its nugget and the region of HAZ close to the nugget are shown in Figs. 13(a) and 13(b), respectively. At a given weld time of 80 cycle the influence of variation in effective current to 6 and 6.8 kA on the microhardness across the weld is shown in Fig. 14. The figure shows that the use of higher effective current of 6.8 kA has weakened the outer region of HAZ considerably due to excess tempering of martensite (Fig. 12) in comparison to that observed in the weld prepared at the effective current of 6 kA.

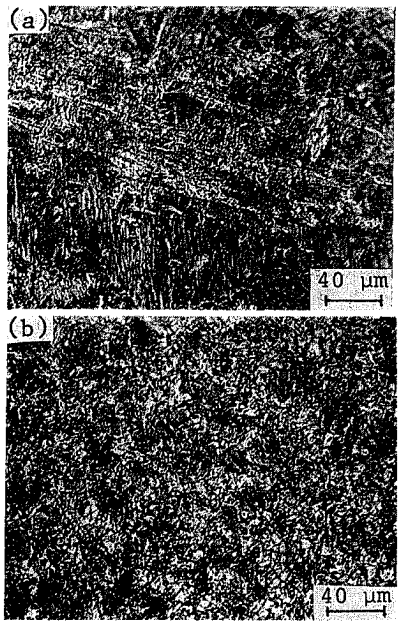

(a) Weld nugget
(b) HAZ close to the weld nugget

Fig. 13.
Microstructures of different region of a weld prepared at effective current of 6 kA and weld time of 80 cycle.

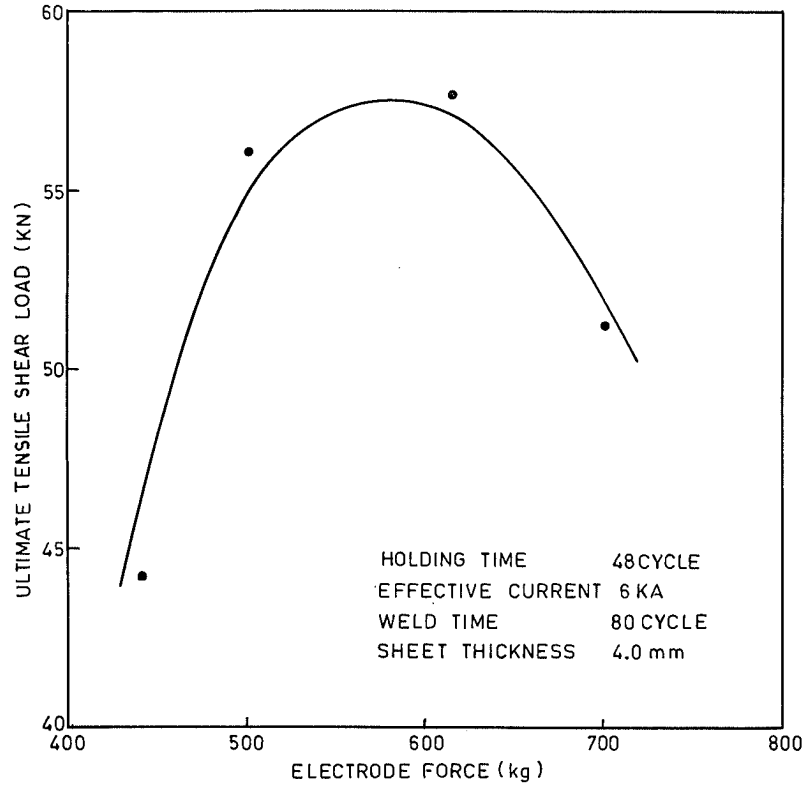

Fig. 15. Effect of variation in electrode force on the ultimate tensile shear load bearing capacity of the weld.

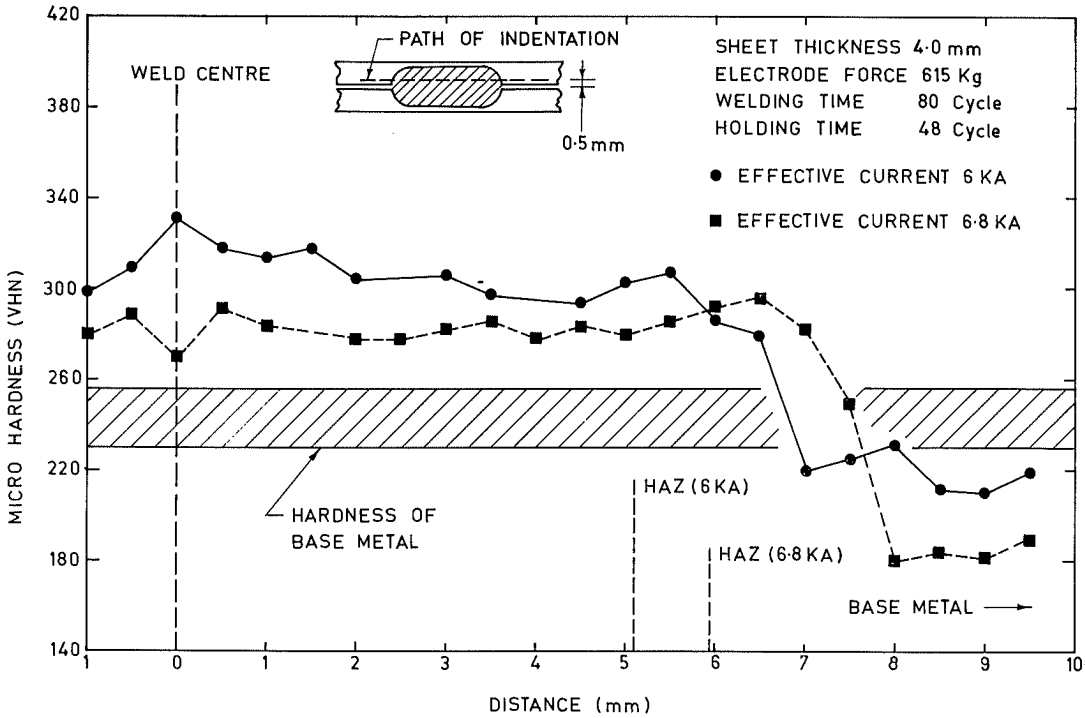

Fig. 14. Microhardness across the weld prepared at different effective current, welding time=80 cycle.

3.4. *Influence of Electrode Force*

The influence of variation in electrode force from 440 to 700 kg on the ultimate tensile shear load bearing capacity of the weld has been shown in Fig. 15, where the effective current and weld time are kept at 6 kA and 80 cycle, respectively. The figure shows that the increase in electrode force from 440 upto 615 kg enhances the tensile shear strength of the weld followed by a decrease in it with a further increase in electrode force to 700 kg. A low electrode force establishes only few contact bridges at the region being welded. Thus, it causes a high local current density resulting into excessive melting/fusion at some spots, giving rise to expulsion from the joint and failure from the interface (Table 2) at a comparatively low tensile shear load. The increase in electrode force produces

more uniform heating and fusion over a larger area and reduces expulsion during welding. At the electrode force of 615 kg the expulsion has been found to be eliminated (Table 2) which has enhanced the nugget strength to a maximum. However, a further increase in electrode force to 700 kg has been found to cause thinning of the nugget by putting a deep impression on the weld surface and thus reducing the weld strength as depicted in Fig. 15.

4. Conclusions

Spot weldability of comparatively thick (4 mm) C–Mn–Cr–Mo dual phase steel sheet is investigated with multiple-impulse resistance welding process. The studies show that the welding parameters such as the effective current and weld time, who primarily govern the thermal cycle of the weld, control the strength of weldment to a great extent by influencing its nugget size as well as the morphology of nugget and HAZ. The use of high effective current of the order of 6.8 kA and a high weld time of 80 cycle and above weakens weldment due to excess tempering of martensite at the outer region of HAZ leading to an early failure from this location. Regarding the strength of weldment the electrode force is also an important criteria found to be considered, which at its low and high level produces expulsion and deep impression at the weld surface respectively thus, weakening the weldment. The optimum parameter for obtaining maximum tensile shear strength of resistance spot welded 4.0 mm thick C–Mn–Cr–Mo dual phase steel has been identified as 6 kA, 80 cycle and 615 kg, respectively.

REFERENCES

1) M. S. Radhid: *SAE Trans.*, **85** (1976), 938.
2) R. G. Davies: *Metall. Trans. A*, **9A** (1978), 671.
3) M. Nishida, K. Hashiguchi, I. Takahashi, T. Kato and T. Tanaka: "Age Hardenable, Low Yield and High Tensile Strength Sheet Steels for Automotives", Proc. 10th Biennial Cong., Sheet Metal Forming and Formability, IDDRG, Univ. Warwick, England, (1978), 211.
4) N. Ohashi, I. Takahashi and K. Hashiguchi: *Trans. Iron Steel Inst. Jpn.*, **18** (1978), 321.
5) K. Kunishige, N. Yamauchi, T. Taka and N. Nagao: "Softening in Weld Heat Affected Zone of Dual Phase Steel Sheet for Automotive Wheel Rim", Proc. Inst. Conf., Detroit, MI, Feb. 28–March 4, (1983), 5.
6) B. Pollard and R. H. Goodenov: SAE Tech. Paper 790006, (1979).
7) B. Pollard: *Weld. J. Res. Suppl.*, (1974), Aug., 348.
8) J. O. Sperle: "Fatigue Strength of Spot Welded High Strength Steel Sheet", Incd. Swedish Symp., Classical Fatigue, ed. by N. G. Ohlson and H. Nordberg, Stockholm, Almqvist and Wiksell Int., ISBN 91-22-00770-9, (1985), 332.
9) T. Irie, T. Kato, A. Tosaka, M. Shinozaki and K. Hashiguchi: SAE Tech. Paper 850118, (1985).
10) J. M. Sawhill: "Spot Weldability of High Strength Sheet Steels—Continuously Heat Treated and Batch Annealed", Proc. Sheet Metal Welding Conf., Am. Weld. Soc., Miami, FL, (1984), Paper-15.
11) J. O. Sperle: *Metal Const.*, **16** (1984), 678.
12) M. Shinozaki, T. Kato, T. Irie and I. Takahashi: SAE Tech. Paper 830032, (1983).
13) J. M. Sawhill and S. T. Furr: SAE Tech. Paper 810352, (1981).
14) R. B. Wilson and T. E. Fine: SAE Tech. Paper 810354, (1981).
15) B. K. Jha, N. S. Mishra and V. Ramaswamy: *Steel India*, **6** (1983), 114.
16) A. J. Brghan: "The Effect of Carbon Content on the Resistance Spot-weldability of As Rolled Dual Phase HSLA Steels", Climax Molybdenum, Michigan R&D Report, L-176-185, (1977).
17) P. C. Gupta, C. L. Raina and B. K. Singh: "Effect of Welding Parameters on the Strength of Steel Spot Welds", Proc. Int. Conf., Weld Tech. in Developing Countries Present Status and Future Needs, Univ. Roorkee, India, (1988), I-135.
18) P. K. Ghosh, P. C. Gupta, R. Avtar and B. K. Jhan: "Weldability of Intercritical Annealed Dual Phase Steel under Resistance Spot Welding Process", *Weld. J.*, AWS, communicated, (1989).
19) P. K. Ghosh and L. Dorn: "Influence of Weld Thermal Cycle on the Properties of Flash Butt Welded Dual Phase Steel", *Schweissen Schneiden*, communicated, (1989).